TÜBİTAK

Turkish Journal of Earth Sciences

http://journals.tubitak.gov.tr/earth/

Research Article

Turkish J Earth Sci
(2023) 32: 75-95

doi:10.55730/1300-0985.1828

Multiphase deformation, fluid flow and mineralization in epithermal systems: Inferences from structures, vein textures and breccias of the Kestanelik epithermal Au-Ag deposit, NW Turkey

Nilay GÜLYÜZ[1,2,*], **Zoe K. SHIPTON**[3], **İlkay KUŞCU**[4]

[1]Department of Geological Engineering, Van Yüzüncü Yıl University, Van, Turkey
[2]Department of Neotectonics and Thermochronology, Institute of Rock Structure and Mechanics, Czech Academy of Sciences, Czech Republic
[3]Department of Civil and Environmental Engineering, University of Strathclyde, Glasgow, UK
[4]Ortaköy Mah. Diğer Sok. No:349/7, Muğla, Turkey

Received: 30.06.2022 • **Accepted/Published Online:** 07.11.2022 • **Final Version:** 19.01.2023

Abstract: We investigate the multiphase deformation, fluid flow, and mineralization processes in epithermal systems by presenting a detailed study of vein textures and breccias of the Kestanelik epithermal Au-Ag deposit, NW Turkey. The mineralization in the deposit is associated with several quartz veins. Fault-hosted veins and mode I veins share many textural and breccia characteristics owing to (i) overprinting of tectonic breccias formed during coseismic rupturing by subsequent coseismic hydrothermal brecciation and (ii) reworking of earlier vein breccia phases by repeated rupturing and hydraulic fracturing events. The spatial distribution of breccias at fault-hosted veins proposes that power of coseismic hydrothermal brecciation is controlled by the distance to the level of boiling within a vein. The brecciation affects the entire vein proximal to the level of boiling; however, it is limited to the footwall contact of the vein more distally at the upper levels of a vein. Varying number of mineralization events for the veins suggests that any individual earthquake event reopened only one or more sealed vein, but not all at once. Fewer mineralization events in fault-hosted veins compared to the mode I veins is either linked to (i) focusing of high fluid flux into the conduits of mode I veins that accommodate more dilation or (ii) reopening of mode I veins owing to the driven of extensional failure under low differential stress. Although fault-hosted veins record fewer mineralization events, they have higher average Au grade (4.106 g/t) compared to that of mode I veins (2.736 g/t). On the other hand, fewer mineralization events in wall rock structures compared to the adjacent faults is attributed to (i) absence or poor development of the damage zone structures in earlier seismic events or (ii) deactivation of them after clogging due to the rotation of the optimum stress field or (iii) their formation as hydraulic extension fractures. This study emphasizes the importance of detailed studies of vein infill for understanding the internal structural evolution of the veins in epithermal deposits that is interest to the geologists within both industry and academic fields.

Key words: Biga Peninsula, earthquake rupturing, hydrothermal, quartz texture, Tethyan metallogenic belt

1. Introduction

Epithermal deposits are shallow deposits (up to 1–2 km depth) formed at low to moderate temperatures (150–300 °C) which are genetically linked to magmatic activities (Hedenquist and Lowenstern, 1994; Sillitoe and Hedenquist, 2003). Faults and fracture systems play a fundamental role in controlling the migration and circulation of hydrothermal fluids in epithermal systems (Hulin, 1929; Buchanan, 1981; Cox et al., 2001; Sibson, 2001; Micklethwaite and Cox, 2004; 2006; Micklethwaite, 2009). In such upper crustal brittle settings, episodic earthquake (seismogenic) rupturing plays a key role in dynamics of stress-states, fluid pressures, and evolution of permeability (Cox et al., 2001; Cox, 2005). Earthquake rupturing causes coseismic dilation in the fault zone that results in a localized fluid pressure drop (Sibson, 1987) that drives intense boiling (flashing) of hydrothermal fluids (Cox et al., 1995; Rhys et al., 2020). These collectively cause rapid deposition of ore and gangue minerals (Buchanan, 1981; Henley, 1985; Brown, 1986; Hedenquist et al., 2000; Henley and Berger, 2000). As a result, open space filling alternates with hydrothermal breccia fill after boiling, and banded veins with crustiform and colloform textures are formed until the hydrothermal system is clogged and complete sealing of structural-vein network takes place. Hydrothermal sealing of structural-vein network causes subsequent fluid pressure build up in the upstream part of the rupture zone (Sibson, 1987; 1992; Cox, 2005)

* Correspondence: nilaygulyuz@yyu.edu.tr

until the next rupturing event that causes dilation and triggers the next boiling process (Hedenquist et al., 2000; Micklethwaite, 2009; Sanchez-Alfero et al., 2016). Repeated cycle at each rupture event results in brecciation of earlier vein phases and supplies a new mineralized cement/filling for the vein system. This results in texturally and compositionally complex nature of the epithermal vein systems (Spurr, 1925; Hulin 1929; Buchanan, 1981; White and Hedenquist, 1995; Hedenquist et al., 2000; Gülyüz et al., 2018; Rhys et al., 2020).

In this regard, understanding the spatio-temporal evolution of epithermal veins in 4-D (x,y,z,t) is significant to document the overall kinematic development and interpretation of epithermal deposits. It is also important in revealing continuity and distribution of different mineralizing phases among individual veins. Since usually only certain generations of vein fill or vein sets can introduce Au-Ag mineralization in epithermal deposits (Rhys et al., 2020), the spatio-temporal evolution of the vein textures and breccias may help to identify the depths and/or zones with higher Au-Ag grade distribution in an individual vein. Moreover, spatio-temporal association of vein textures and breccias with respect to deformation in faults or shear zones is critical for understanding the 3-D architecture of the paleo-hydrothermal plumbing system that is a part of the exploration process (Cox, 2020).

Understanding and use of the complicated 4D evolution of coupled flow and fracture systems like epithermal systems requires identification of the structures and vein textures preserved in the rock record (e.g., Hulin, 1929; Tarasewicz et al.,2005; Woodcock et al., 2007; Caine et al., 2010; Frenzel and Woodcock, 2014; Gülyüz et al., 2018; Masoch et al., 2019; McKay et al., 2019).

The epithermal ore-vein and quartz textures have been the subject of numerous studies aiming to understand physico-chemical evolution of hydrothermal fluids (e.g., Dowling and Morrison, 1989; Saunders, 1994; Dong et al., 1995; Simmons et al., 2005). However, only a few studies (Moncada et al., 2012; Shimizu, 2014) focus on the association of various epithermal quartz textures with their fluid inclusion characteristics in order to reveal the genetic association between these textures and the precious metal precipitation processes, and physiochemical conditions during their formation. There are also some limited studies (Strujkov et al., 1996; Chauvet et al., 2006; Chauvet, 2019) interpreting the changes in quartz textures in relation to structural control on vein formation.

In this contribution, we focused on the Kestanelik deposit, an operating well exposed low sulphidation epithermal Au-Ag vein system in the Biga peninsula (Çanakkale, NW Turkey). Despite that epithermal deposits are characterized commonly by laminated textural features and there also exists other processes of formation than explosion or brecciation, banding, and laminated textures are lacking or very rare in the Kestanelik veins. These veins are frequently characterized by multiphase breccia infill. The present work presents field and petrographic vein infill data from the Kestanelik deposit with the topics of understanding the spatio-temporal association between texturally different quartz generations that seal the structures, earthquake rupturing, and hydrothermal eruption events which restore permeability. In this sense, this study conducts detailed dissection of the textural variations in space (x,y,z) and time (t) in multiple epithermal vein system.

The study sheds light on the multiple pulses of hydrothermal fluid flow and associated quartz generations and mineralization processes coupled to repeated cycles of seismic rupturing and boiling events in epithermal systems as a case study at the Kestanelik deposit. It also emphasizes the importance of identifying different generations of quartz in delineating the formation, continuity, and distribution of mineralization stages within vein system(s) in hydrothermal ore deposits.

2. Kestanelik epithermal Au-Ag deposit

The Kestanelik Au-Ag deposit is located in the Biga Peninsula, NW Turkey approximately 45 km northeast of Çanakkale (Figures 1a, 1b). Paleozoic metamorphic and ophiolitic rocks form the basement in the Biga peninsula, and are cut by various Eocene to Miocene plutons covered by Cenozoic volcanic and sedimentary rock units (Okay et al., 1996) (Figure 1b). Starting from the Middle Eocene, extensive magmatism that shifted from calc-alkaline to alkaline in character in middle Miocene from north to south, prevailed in NW Turkey (Altunkaynak and Genç, 2008; Kuşcu et al., 2019).

The Kestanelik is a low sulphidation epithermal deposit hosted by hydrothermally altered mica schist and quartz-feldspar-hornblende (QFH) porphyry (Gülyüz et al., 2018). Based on the presence of bladed quartz after calcite, complex infilling, low base metal, and total sulphide (2%–4%) contents, Gülyüz et al. (2020) defined the deposit as low sulphidation epithermal system. Adularia, one of the most significant mineral in low sulphidation epithermal systems, has not been identified in the Kestanelik that is attributed to the absence of potassium in the calc-alkaline host rock QFH porphyry (Gülyüz et al., 2020). Hydrothermal alteration is especially conspicuous around the veins in the hosted porphyry, and is commonly represented by intermediate argillic alteration (Gülyüz et al., 2020). A middle Lutetian-early Priabonian time interval (44-37 Ma) is proposed for the age of the mineralization based on the youngest sedimentary cover unconformably overlying the veins and Eocene QFH porphyry that cross cuts the metamorphic rocks (Gülyüz et al., 2020).

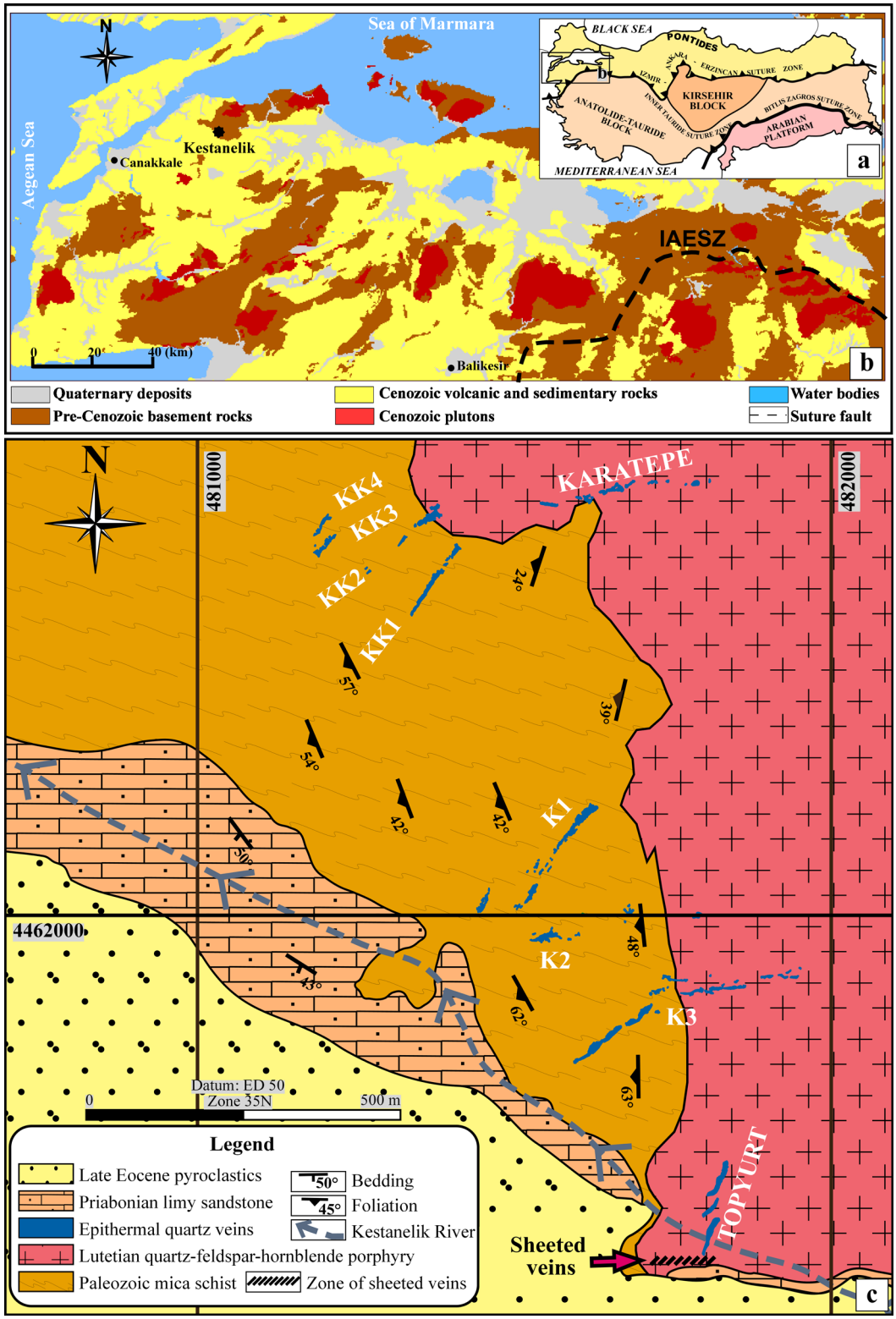

Figure 1. (a) Major tectonic terranes of Turkey (simplified from Okay and Tüysüz 1999). (b) Simplified geological map of the Biga Peninsula (IAESZ: İzmir-Ankara-Erzincan Suture Zone) with the location of the study area (modified from Türkecan and Yurtsever, 2002). (c) Geological map of the study area, Kestanelik vein system (from Gülyüz et al. 2018).

Veins of the deposit are characterized by several quartz textures including pseudo-bladed quartz, colloform to crustiform quartz, and comb to cockade vein textures and hydrothermal breccias. The absence of silica sinter, the diagnostic paleosurface indicator of LS epithermal systems (Hedenquist et al., 2000), indicates that the veins have been subjected to erosion and only subsurface parts of them are exposed (Gülyüz et al., 2020). A general change of dominant quartz textures from colloform chalcedony in the north through to crystalline quartz textures in the south suggests a level of erosion and paleodepth in the vein system increase from the north to the south (Gülyüz, 2017).

The veins contain quartz, chalcedony, and calcite as the common gangue minerals. Breccias are cemented by contemporaneous hypogene hematite and crypto- to micro-crystalline quartz. Apart from the hypogene hematite, supergene iron oxides (hematite and goethite) are also observed as filling of fractures and vugs between breccia-related clasts and fragments (Gülyüz et al., 2020). Native gold is the prime commodity along with silver and disseminated pyrite at the deposit. Most of the gold is microscopic and is observed as dendritic pale-coloured native gold flakes within (i) the hematite cemented breccia and (ii) cavities infilled by goethite. Yet, very limited native gold flakes are visible at the intersections with bonanza grades above ~60 g/t Au where goethite prevails due to supergene oxidation prevails (Gülyüz et al., 2020). Silver is generally low with Ag/Au ratio close to 1, and elevated silver values up to 85g/t are associated with gold (Gülyüz et al., 2018; 2020). No work on the mineralogy and Ag-bearing mineral assemblages has been conducted for the moment. Yet, the changes in the Ag/Au ratios are variable and are ascribed to physico-chemical conditions of ore-forming fluids (Gülyüz et al., 2020). In that sense, the Kestanelik is considered to be an example of low Ag-bearing epithermal Au-Ag deposits such as those in Japan (Ag/Au ratios lower than 10; Shikazano and Shimizu, 1987).

NE-SW oriented compression due to the collision and further convergence after the closure of the northern branch of the Neo-Tethys Ocean in NW Turkey in the Late Cretaceous-Early Eocene is responsible for the formation of structures hosting mineralized veins at Kestanelik (Gülyüz et al., 2020). The major mineralized veins at the Kestanelik deposit, from north to south are, the Karatepe, KK4, KK3, KK2, KK1, K1, K2, K3, and Topyurt veins (Figure 1c). The veins generally have along-strike lengths of several tens to several hundreds of m and their widths vary between 0.8 and 13.6 m on the surface (Figure 2a). Based on their attitudes, the mineralized veins are grouped into two sets: E-W trending ones (Karatepe, K2 and K3 veins), and NE-SW to NNE-SSW ones (KK1, KK2, KK3, KK4, K1, and Topyurt veins). According to the paleostress analysis of Gülyüz et al. (2018), E-W trending veins are hosted by left-lateral strike slip faults and are classified as fault-hosted veins, whereas NE-SW to NNE-SSW veins, except the Topyurt vein, are formed by mode I fractures and are termed as mode I veins.In addition, the Topyurt vein is hosted by right-lateral en-echelon brittle shear zone (Gülyüz et al., 2018; Figure 3a). As obtained from the 3D modelling study, the average Au grades of the major veins vary between 0.461 g/t (Karatepe vein) and 6.943 g/t (K3 vein western section) (Gülyüz et al., 2018). In addition, the average gold content of the fault-hosted veins is 4.106 g/t, while those of mode I veins are 2.736 g/t. The margins of the Karatepe and Topyurt veins are surrounded by wall rock quartz veins on the surface (Figure 2b). These veins are subvertical, oriented almost NE-SW, and generally curve towards the major Karatepe and Topyurt veins. Their width varies between 4 and 26 cm, and 3 and 20 cm on the surface around the Karatepe and Topyurt veins, respectively (Gülyüz et al., 2018). These wall rock veins are considered as extensional damage zone veins developed around the fault-hosted Karatepe vein and in Topyurt en-echelon brittle shear zone. The extensional damage zone veins are also observed around the fault-hosted K3 and K2 veins in drill cores. In addition to the major fault-hosted, mode I veins, and extensional damage zone veins; almost NE-SW trending 3–15 cm thick subvertical and subparallel extensional sheeted quartz veins (Figure 2c) are observed at the deeply incised valley floor of the Kestanelik River and are classified as extensional sheeted veins (Gülyüz et al., 2018). The extensional sheeted veins have very high Au grades and a sample collected from these veins returned 419 g/t Au, the highest Au grade of the deposit to date (Gülyüz et al., 2020).

Multiple phases of mineralization at the Kestanelik deposit are stated by Gülyüz et al. (2018). The multiphase mineralization is related to repeated permeability development and fluid flow induced primarily by coseismic (earthquake) rupturing and subsequent intense boiling (flashing) events, while hydraulic fracturing and transient local stress variation are given as the secondary permeability enhancement mechanisms (Gülyüz et al., 2018). During any coseismic rupturing event, reopening of the sealed E-W trending fault-hosted veins occurs at the contact between the vein footwall (FW) and wall rock. Although the coseismic boiling-induced brecciation obliterated much of the evidence of shearing within the veins, it is rarely preserved and observed at the FW margins as microscale tectonic breccias (K3 vein) and cataclasite (Karatepe vein) (Gülyüz et al., 2018). On the other hand, reopening of the sealed NE-SW trending mode I veins and Topyurt en echelon veins occurs along either margin (FW or HW) of the veins (Gülyüz et al., 2018; Figure 3b).

Figure 2. (a) Field exposure of major quartz veins; KK1 vein. (b) Field exposure of wall rock quartz veins within the damage zone of the Karatepe vein. (c) Sheeted quartz veins at the valley floor of the Kestanelik River.

The deposit is one of the important ore deposits discovered in late 1992 with prolonged exploration-drilling history by Eurogold and Chesser Resources between 2009–2016. It has been operated as an active open pit mine by Tümad Madencilik since November 2017. It has a resource of 7.15 million t of ore @ 1.85 Au and 1.86 g/t Ag, with Au/Ag ratio of 0.99 (Tümad Madencilik ve Sanayi A.Ş., n.d.).

3. Materials and methods

Quartz textures and breccia types of nine major veins (fault-hosted and mode I veins) together with extensional sheeted quartz veins and extensional damage zone (wall rock) veins were examined macroscopically at the field from outcrops as possible as intense weathering and vegetation allowed. Also, drill cores from 254 diamond cuts, and chips from 139 reverse circulation holes were used in macroscopic works.

Petrographical analyses were performed on 58 thin sections on core and chip samples selected from the Karatepe, KK1, and K3 veins since these veins contain multiple quartz generations with different textures, and are associated to the gold mineralization occurrences in different sectors of the study area characterizing different depths and gold assays. The sampling strategy involves the collection of samples (i) with textures having cross-cutting relationships, (ii) from hanging wall (HW) and footwall (FW) margins of the veins, and (iii) from different depths of the same vein. This enables to (i) determine mineralization phases, (ii) recognize structural-textural relationships, and (iii) correlate possible textural changes with depth.

The characterization of quartz textures along with their cross-cutting relationships, and of breccia types based on clast types, matrix types, cement types, roundness, and sorting of clasts is also regarded during our study.

4. Results

4.1. Textural and breccia characteristics of the Kestanelik mineralized veins

Textural and breccia characteristics of the Kestanelik mineralized veins are summarized to reveal quartz generations and associated mineralization(s) if multiple,

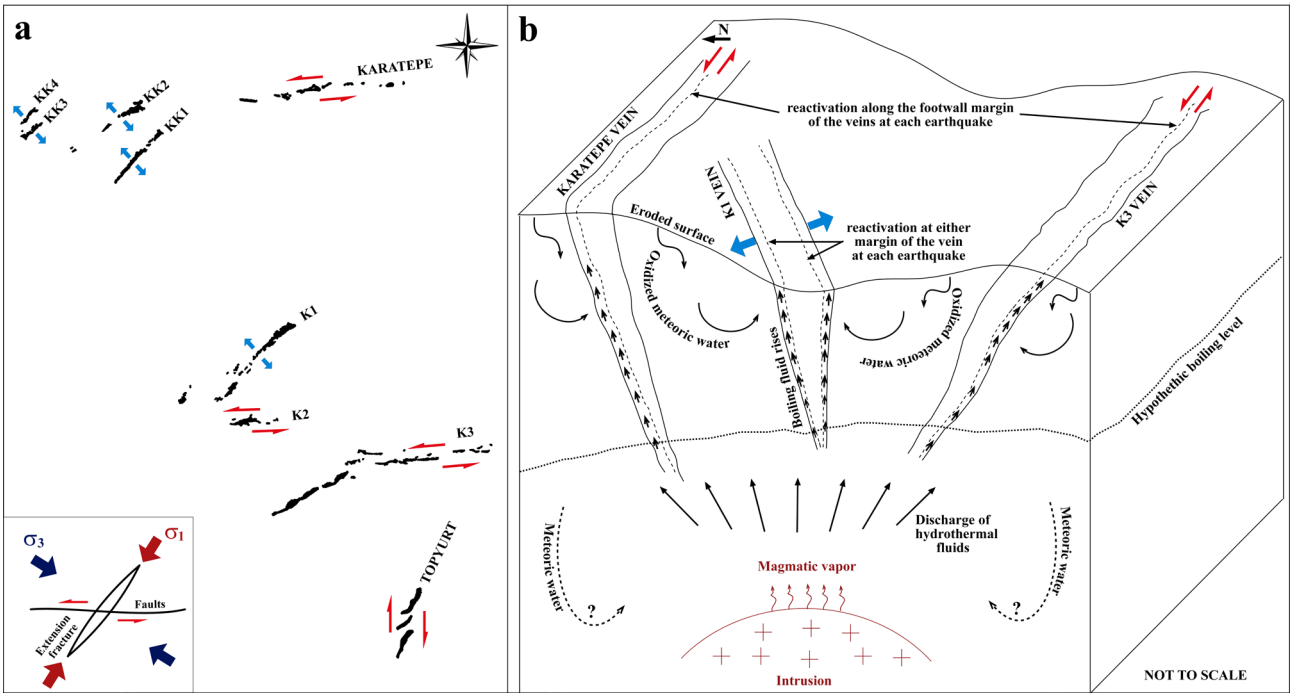

Figure 3. (a) A hypothetical model showing the opening of the structures hosting the Kestanelik major mineralized quartz veins based on the determined principal stress directions at Gülyüz et al. (2018) (b) A conceptual model for the repeated reactivation and opening of clogged veins and associated fluid flow and mineralization. It should be noted that the K3 vein represents the fault-hosted veins (except the Karatepe vein), whereas the K1 vein represents the mode I veins of the Kestanelik (modified from Gülyüz et al., 2018).

and constrain the relative timing of mineralization and brecciation. They have been divided in four groups: (1) E-W trending fault-hosted veins, (2) NE-SW to NNE-SSW trending mode I veins, (3) NNE-SSW trending Topyurt vein, and (4) extensional damage zone veins and extensional sheeted veins.

4.1.1. E-W trending fault-hosted veins

Karatepe, K2, and K3 veins are characterized by two main quartz textures: chalcedony and crystalline quartz. The chalcedonic quartz is identified at relatively shallower depths close to the surface. The Karatepe vein with chalcedonic quartz displays two textures: (1) cockade and (2) crustiform textures (Figure 4a). Very thin crusts of chalcedony rimming the clasts of hydrothermally altered QFH porphyry forms the cockade textured chalcedony (Figure 4b), and represents the phase 1 (p1) quartz generation and associated gold mineralization of the vein. On the other hand, the thinly-laminated to thinly-banded chalcedony deposited within the veinlets along the micro fractures form the crustiform textured chalcedony at the footwall margin of the Karatepe vein (Figures 4a and 4c). It cut across the cockade chalcedony (p1), and forms the phase 2 (p2) quartz generation and mineralization in the vein. Although these textures are examined from 14 drill cores representing different levels of the Karatepe vein (394 m above sea level (asl)-238.2 m asl), no change is observed with depth.

The crystalline quartz is identified at deeper levels than the chalcedonic quartz, and is hosted by K2 and K3 veins. The crystalline quartz at K2 and K3 veins displays (i) saccharoidal (Figure 4d), (ii) pseudobladed commonly in the lattice bladed (Figure 4e), (iii) colloform (Figure 4f), and (iv) massive (Figure 4h) crypto- to micro-crystalline quartz. Saccharoidal, pseudobladed and massive quartz textures are commonly synchronous (Figures 4g and 4h) and represent the phase 1 (p1) quartz generation and mineralization in these veins. The massive crypto- to micro-crystalline quartz is also seen as accompanied by hypogene hematite forming quartz±hematite cement within matrix-supported polymictic breccias (Figure 5a). The massive crypto- to micro-crystalline textured quartz and hypogene hematite were formed by mixing ascending hydrothermal fluids with oxidized meteoric groundwater (Gülyüz et al., 2020), and represent the phase 2 (p2) quartz generation and mineralization (Figure 5a). These quartz±hematite occurrences exhibit colloform banding where they become crypto-crystalline in the K3 vein (Figure 4f). Examination of the textures from the drill cores of different levels of the K3 vein (from 363 m asl to 183.4 m asl) shows no change of textures with depth.

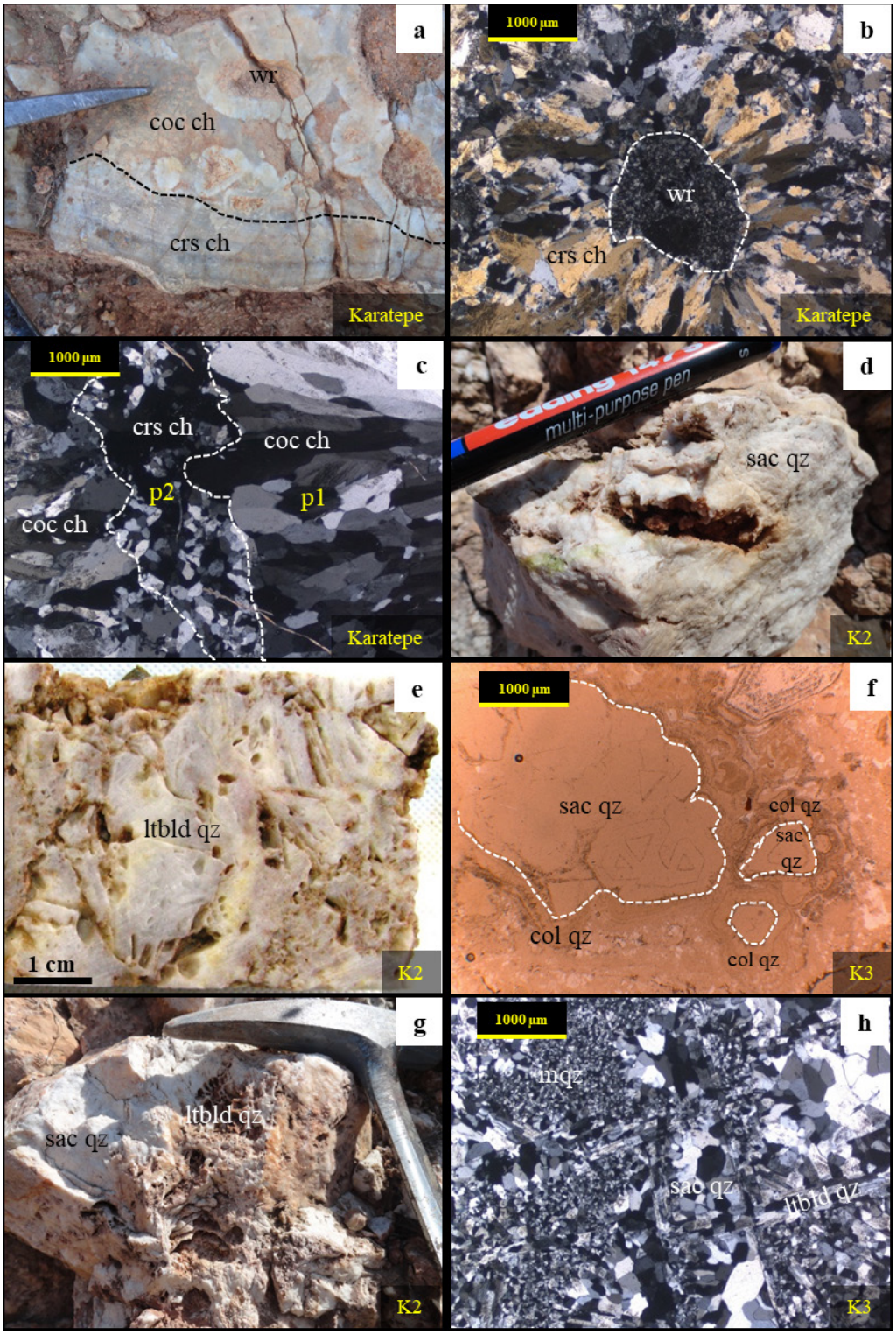

Figure 4. (a) Cockade chalcedony (coc ch) and crustiform chalcedony (crs ch) on outcrop of the Karatepe vein. (b) Crustiform chalcedony rimming a clast of altered wall rock (wr) and forming the cockade chalcedony (crossed polars image from a drill core sample at KED-16 124 m cutting the Karatepe vein). (c) A veinlet of crustiform chalcedony cutting the cockade chalcedony (crossed polars image from a drill core sample at KED-16 124 m cutting the Karatepe vein). (d) Saccharoidal quartz (sac qz) on outcrop of the K2 vein. (e) Lattice bladed quartz (ltb qz) in a drill core cutting the K2 vein (KED 161–15.3 m). (f) Colloform quartz (col qz) lining euhedral saccharoidal quartz crystals (plane polarized light image from an outcrop sample of the K3 vein at 280 m). (g) Synchronous saccharoidal and lattice bladed quartz on the K2 vein outcrop. (h) Synchronous saccharoidal, lattice bladed and massive quartz (mqz) (crossed polars image from an outcrop sample of the K3 vein at 280 m asl).

The brecciation is remarkable in the K2 vein and K3 veins whereas no breccia is observed at the Karatepe vein except cockade-textured breccias (Figure 4a). Three different types of breccia are identified; (1) Matrix-supported polymictic breccias, 2) crackle to mosaic breccias cemented by quartz±hematite, and (3) chaotic polymictic breccias cemented by quartz±hematite. The matrix-supported polymictic breccias contain poorly-sorted, angular to subangular clasts of schist and QFH porphyry cemented by (synchronous) saccharoidal-lattice bladed-massive crypto- to micro-crystalline quartz with a matrix ratio over 70% (Figures 5b and 5c). These breccias are found either close to the hanging-wall (HW) margin of the veins or in the vein cores, and commonly predominate close to the upper levels of the veins. The crackle-to-mosaic breccias cemented by quartz± hematite are also matrix-supported breccias that consist of poorly- to well-sorted, angular to subrounded clasts derived mostly from the earlier vein (Figure 5d) and less commonly from schist and QFH porphyry (Figure 5e). The clasts derived from the veins contain saccharoidal, lattice bladed, and massive crypto- to micro-crystalline quartz (Figure 5d). The clasts show little or no rotation (Figures 5d and 5e). The matrix is always massive crypto- to micro-crystalline quartz±hematite with a variable degree of matrix ratio ˜20%–80% (Figures 5d and 5e). These breccias are either observed close to the footwall margins of the veins or constitute the entire vein infill. The chaotic polymictic breccias cemented by quartz±hematite are clast- to matrix-supported breccias composed of poorly-sorted, angular to subrounded polymictic clasts derived from veins with different quartz textures. Clasts display massive crypto- to micro-crystalline (Figure 5f), lattice bladed (Figure 5g), and saccharoidal (Figure 5h) quartz textures. The matrix is massive micro-crystalline quartz-hematite with a ratio of <20% (Figures 5f, 5g, 5h). These breccias are only found at the upper levels of the K3 vein (from the top –363 m asl- to the level 280 m asl).

4.1.2. NE-SW to NNE-SSW trending mode I veins

Textures identified at the KK1, KK2, KK3, KK4, and K1 mode I veins include (i) saccharoidal (Figure 6a), (ii) pseudobladed in the lattice bladed form (Figures 6b and 6d), and (iii) massive crypto- to micro-crystalline quartz (Figure 6c). Saccharoidal and lattice bladed quartz are synchronous (Figure 6d) in these veins. Massive crypto- to micro-crystalline quartz is associated with hematite where it cements the clasts of earlier quartz generations (Figure 6e). Macroscopic and petrographic observations of drill cores intersecting different depths of the KK1 vein (from 340 m asl to 250.8 m asl), KK2 vein (from 273.6 m asl to 229.4 m asl), and K1 vein (from 290 m asl to 229.4 m asl) showing the same texture and thus indicating that quartz textures of the veins do not vary with depth.

Four different quartz generations and associated mineralization with distinctive textures are identified at the KK1 and KK3 vein; based on cross-cutting relationships of the textures. These are: (1) massive micro-crystalline quartz (Figure 6f) that refers to phase 1 (p1) quartz generation, (2) saccharoidal quartz (Figure 6g and 6h) referring to phase 2 (p2), (3) synchronous saccharoidal and pseudobladed quartz (Figures 6f, 6g, 6h) referring to phase 3 (p3) and (4) massive micro-crystalline quartz-hematite (Figure 6h) referring to phase 4 (p4). On the other hand, 3 different quartz generations and associated mineralization phases (p1 to p3) are differentiated from the KK2, KK4, and K1 veins; (1) massive crypto-crystalline quartz (Figure 7a) that refers to phase 1 (p1), (2) synchronous lattice bladed and saccharoidal quartz (Figure 7b) referring to phase 2 (p2), (3) massive micro-crystalline quartz-hematite (Figure 7c) referring to phase 3 (p3).

Three different breccia types are identified from the mode I veins; (1) matrix-supported monomictic breccias, (2) crackle to mosaic breccias cemented by quartz-hematite, and (3) chaotic polymictic breccias cemented by quartz-hematite. The matrix-supported monomictic breccias contain poorly- to well-sorted angular to subangular clasts of wall rock schist supported by saccharoidal and lattice bladed quartz with a matrix ratio over 50% (Figures 6a, 7d, and 7e). They are found close to the either HW or FW margin of the veins as fragments within later generations of breccias. The crackle to mosaic breccias cemented by quartz-hematite have jigsaw-fit and poorly- to well-sorted angular to subrounded clasts always cemented by massive micro-crystalline quartz-hematite with a variable degree of matrix ratio ˜20%–70%. The clasts consist mainly of saccharoidal quartz (Figure 7f), earlier vein infill(s) and wall rock schist (Figures 7g and 7h). The chaotic polymictic breccias cemented by quartz-hematite are also termed as matrix-supported breccias, and are composed of polymictic, angular to subrounded and poorly-sorted (Figure 8a) clasts of earlier vein infills with different quartz textures. They are cemented by massive micro-crystalline quartz-hematite. These breccias have cement ratios always less than 50%, and are generally more predominant at the upper levels of the veins.

4.1.3. Topyurt vein system

Topyurt vein system consists of three subparallel NNE-SSW trending veins, and three phases of quartz generation and associated mineralization phases (p1 to p3) are identified in this vein system; (1) massive micro-crystalline quartz rimming the subangular to rounded clasts of wall rock QFH porphyry (Figures 8b and 8c) forming the cockade texture generated during phase 1 (p1), (2) orange colored iron oxide-bearing (?) massive micro-crystalline quartz (Figure 8c), generated during phase 2 (p2) and (3) massive micro-crystalline quartz accompanied by

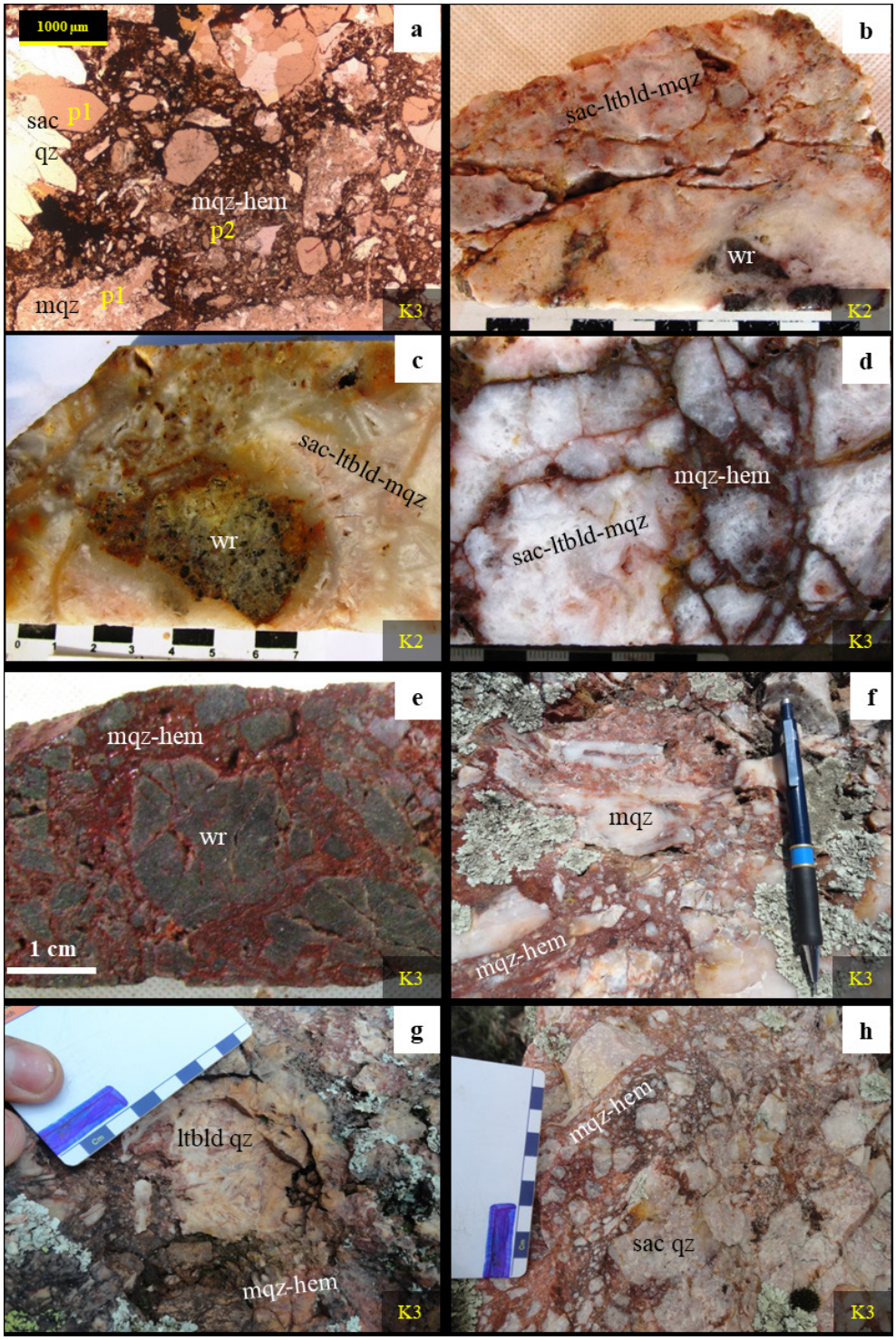

Figure 5. (a) Breccia with clasts and grains of saccharoidal (sac qz) and massive quartz (mqz) cemented by massive quartz-hematite (mqz-hem) (plane polarized light image from a drill core sample at KED-20 30.1 m cutting the K3 vein). (b) Breccia of wall rock (wr) schist cemented by synchronous saccharoidal, lattice bladed (ltbld qz) and massive quartz as fragment in a later generation of breccia in a drill core cutting the K2 vein (KED-46 2.3 m). (c) Breccia of wall rock (wr) QFH porphyry cemented by synchronous lattice bladed and massive quartz in a drill core cutting the K2 vein (KED-34 47 m). (d) Crackle breccia of synchronous saccharoidal-lattice bladed and massive quartz cemented by massive quartz-hematite in a drill core cutting the K3 vein (KED-14 70.5 m). (e) Mosaic breccia of wall rock schist cemented by massive quartz-hematite in a drill core cutting the K3 vein (KED-72 79.7 m). (f) Chaotic breccia of massive quartz cemented by massive quartz-hematite on outcrop of the K3 vein. (g) Crackle to chaotic breccia of lattice bladed quartz cemented by massive quartz-hematite on outcrop of the K3 vein. (h) Chaotic breccia of saccharoidal quartz cemented by massive quartz-hematite on outcrop of the K3 vein.

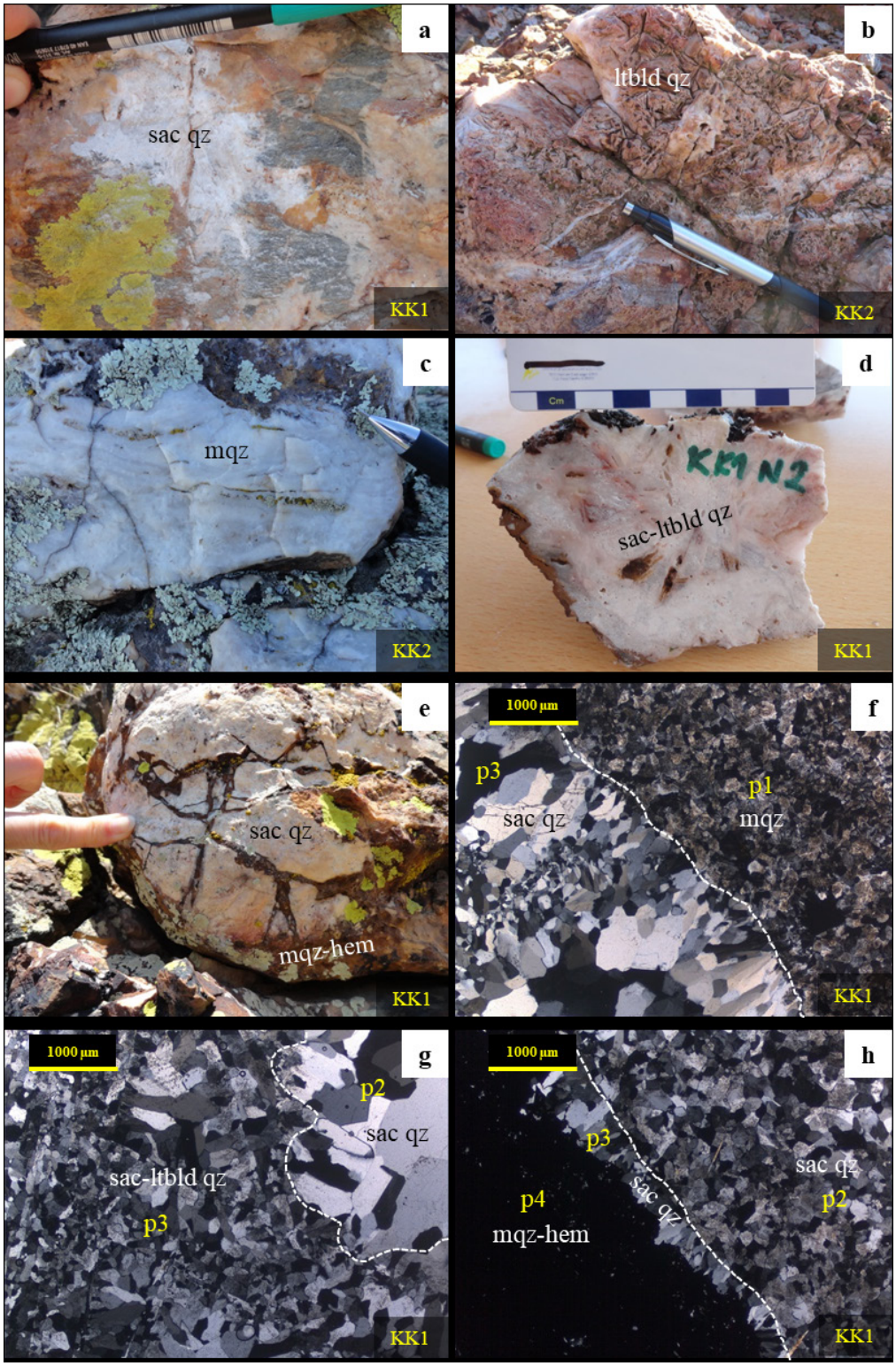

Figure 6. (a) Saccharoidal quartz (sac qz) cementing the clasts of wall rock schist on the KK1 vein outcrop. (b) Lattice bladed quartz (ltbld qz) on the KK2 vein outcrop. (c) Massive quartz (mqz) on the KK1 vein outcrop. (d) Synchronous saccharoidal and lattice bladed quartz from the KK1 vein outcrop. (e) Crackle breccia of saccharoidal quartz cemented by massive quartz-hematite on the KK1 vein outcrop. (f) Massive quartz cut by saccharoidal quartz (crossed polars image from an outcrop sample of the KK1 vein at 324 m). (g) Synchronous saccharoidal and lattice bladed quartz cutting saccharoidal quartz (crossed polars image from an outcrop sample of the KK1 vein at 312 m). (h) Massive quartz-hematite cementing earlier phases of saccharoidal quartz (crossed polars image from an outcrop of the KK1 vein sample at 324 m).

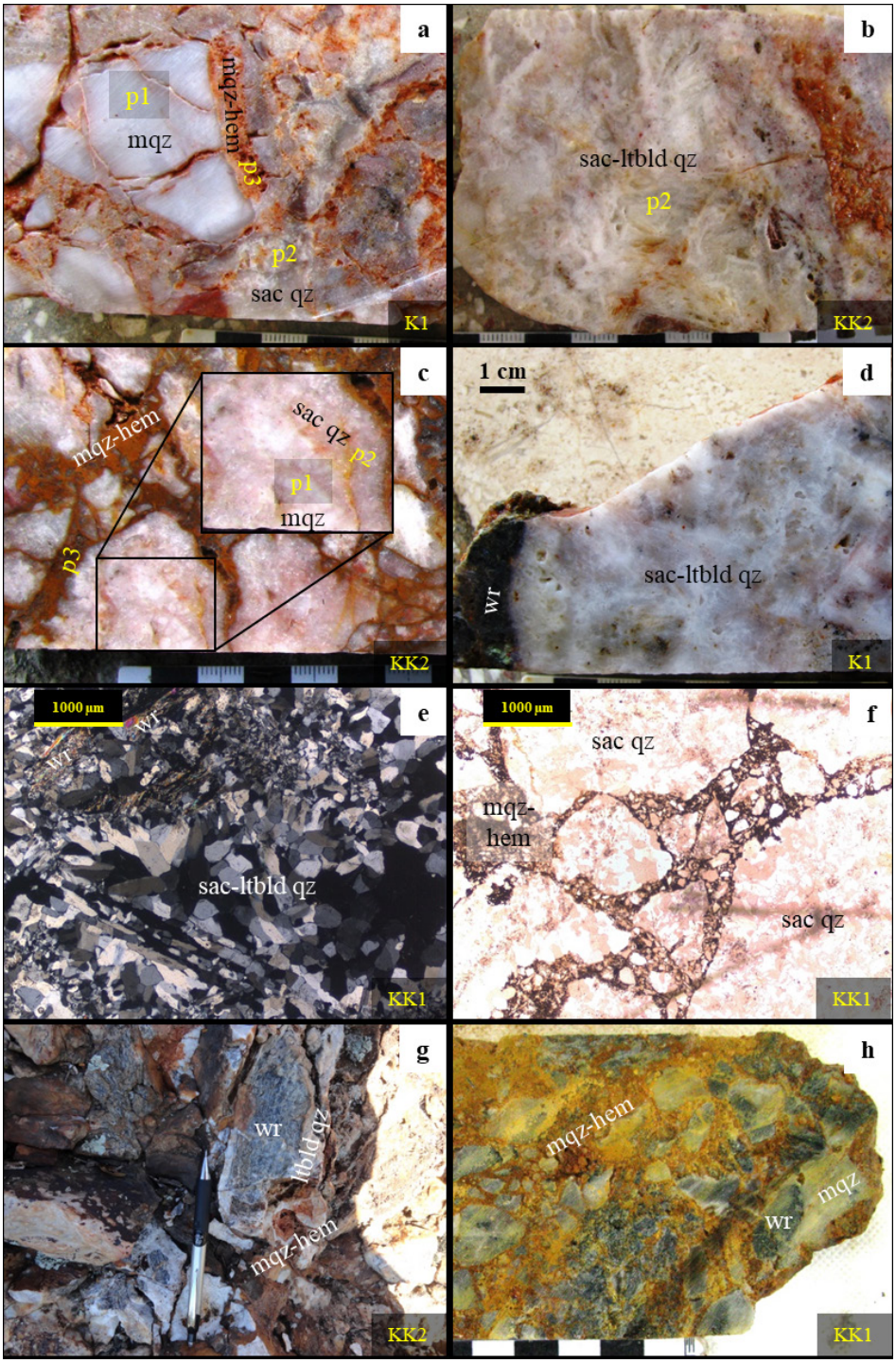

Figure 7. (a) Crackle to mosaic breccia of saccharoidal (sac qz) and massive quartz (mqz) plus a matrix of quartz-hematite (mqz-hem) in a drill core cutting the K1 vein (KED-5 35.5 m). (b) Synchronous saccharoidal and lattice bladed quartz (ltbld qz) in a drill core cutting the KK2 vein (KED-9 7.8 m). (c) Crackle breccia with massive quartz-hematite cementing the clasts of earlier breccia of saccharoidal quartz cementing white massive quartz in a drill core cutting the KK2 vein (KED-1 11.6 m). (d) Synchronous saccharoidal and lattice bladed quartz cementing the clasts and fragments of wall rock (wr) schist in a drill core cutting the K1 vein (KED-5 36.5 m). (e) Synchronous saccharoidal and lattice bladed quartz replacing and cementing the angular clasts of wall rock schist (crossed polars image from an outcrop sample of the KK1 vein at 324 m). (f) Crackle to mosaic breccia with clasts of saccharoidal quartz cemented by massive quartz-hematite (plane polarized light image from a drill core sample at KED-7 13.1 m cutting the KK1 vein). (g) Mosaic breccia with clasts of earlier vein infill containing wall rock schist clasts surrounded by lattice bladed quartz cemented by massive quartz-hematite on the outcrop of the KK2 vein. (h) Mosaic breccia of wall rock schist and massive quartz cemented by massive quartz hematite in a drill core cutting the KK1 vein (KED-105 77.3 m).

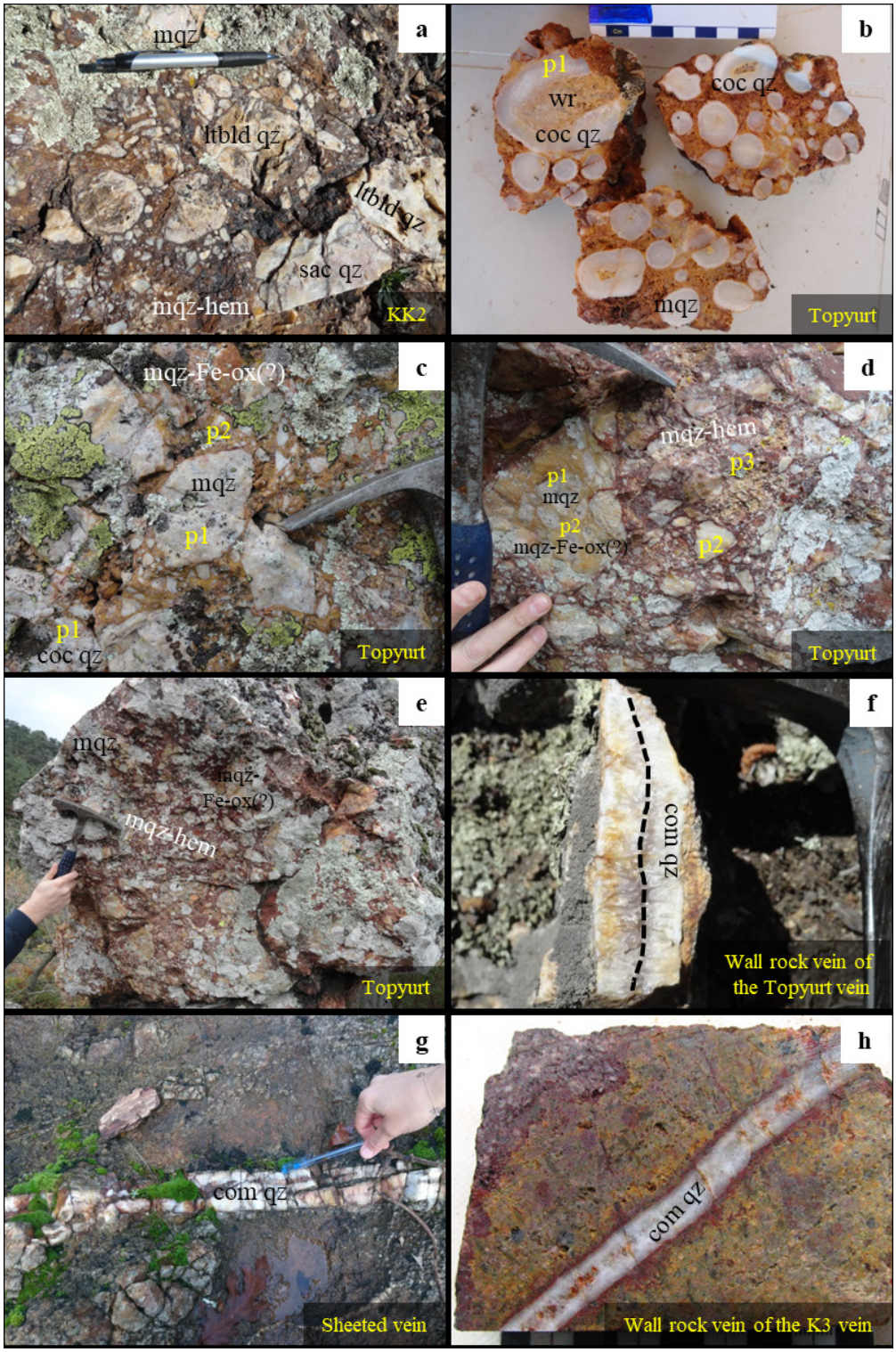

Figure 8. (a) Chaotic breccia of saccharoidal (sac qz), lattice bladed (ltbld qz) and massive quartz (mqz) cemented by massive quartz-hematite on the outcrop of the KK2 vein. (b) Massive (mqz) to cockade (coc qz) quartz enclosing the clasts of wall rock (wr) QFH porphyry from the outcrop of the Topyurt vein. (c) Orange colored iron oxide bearing (?) massive quartz (mqz-Fe-ox(?)) cementing the clasts of mostly cockade massive quartz on the outcrop of the Topyurt vein. (d) Breccia with clasts of orange colored iron oxide bearing (?) massive quartz and earlier vein infill cemented by massive quartz-hematite on the outcrop of the Topyurt vein. (e) Mosaic to chaotic breccia of massive quartz and orange colored iron oxide bearing (?) massive quartz cemented by massive quartz-hematite on the outcrop of the Topyurt vein. (f) Comb quartz (com qz) in the wall rock vein around the Topyurt vein. (g) Sheeted veins having comb quartz. (h) Wall rock vein having comb quartz in a drill core intersecting the K3 vein (KED-59 56.4 m).

hematite cementing the clasts within breccias of earlier quartz generations (Figure 8d), generated during phase 3 (p3).

Brecciation is very prominent in the Topyurt veins. Mosaic to chaotic breccias are matrix-supported and composed of poorly-sorted angular to subrounded clasts of earlier vein infills. The matrix is massive micro-crystalline quartz-hematite with a ratio of ˜40% (Figures 8d and 8e).

4.1.4. Extensional damage zone veins and sheeted veins

Damage zone veins peripheral to the fault-hosted veins, and the sheeted veins at the valley floor are both extensional (Gülyüz et al., 2018) and share the same textural characteristics. These veins are composed of syntaxially grown macro-crystalline comb-textured quartz crystals (Figures 8f, 8g, and 8h). The wall rock veins have equigranular infill, and are composed of light-colored amethystine quartz (Figure 8f), whereas sheeted veins are composed of milky white quartz crystals (Figure 8g).

5. Discussion

5.1. Internal evolution of the major veins by multiphase deformation, fluid flow and mineralization

Integration of the vein kinematics and permeability enhancement mechanisms presented in Gülyüz et al. (2018), and the characteristics and distribution of breccias within the veins presented in this study and also summarized in Figure 9, gives way to suggest hypotheses for 4D (x,y,z,t) internal evolution of the fault-hosted (K2 and K3) and mode I veins during epithermal mineralization (Figure 10 and 11) which are explained below.

During an earthquake event, reopening of sealed fault-hosted veins along the vein footwall-wall rock contact (Gülyüz et al., 2018) causes tectonic brecciation of both (i) earlier vein infill and (ii) wall rock along the FW margin of the vein (Figure 10a). Coseismic fluid pressure drop triggers vigorous boiling (flashing) of hydrothermal solutions, which is evident from the common occurrence of pseudo-bladed quartz and hydrothermal crackle breccia in the Kestanelik veins (Gülyüz et al., 2018). Crackle to mosaic breccias with massive quartz±hematite (p2) cementing angular clasts of earlier vein phase (p1) (Figure 5d) and wall rocks (Figure 5e) indicate overprinting of tectonic breccias by hydrothermal brecciation (Figures 10a and 10c).

Flashing following the coseismic rupture does not cause overall brecciation of entire vein infill (Figure 10). At the upper levels of the veins, flashing causes brecciation of wall rock adjacent to the footwall and partial brecciation of previous vein infill close to the footwall of the vein (Figures 10a and 11). In this case, postbrecciation flow is limited to only FW margin of the vein as earlier vein infill is preserved close to the hanging wall of the vein, and it is evidenced by the breccias with wall rock clasts cemented by earlier quartz generations (Figure 5c) close to the HW of the veins and in the vein cores (Figures 10a and 11). At the lower levels of the veins, flashing causes complete brecciation of the vein infill and derivation of wall rock from the vein hanging wall and footwall (Figures 10a and 11). At these levels, the flow is through the entire vein and it is evidenced by crackle to mosaic breccias of earlier vein infill and/or wall rocks cemented by massive micro-crystalline quartz±hematite observed through the entire infill of the vein (Figures 5d, 5e, and 11). Little or no rotation of the clasts within the crackle to mosaic breccias (Figures 5d, 5e, and 11) is interpreted to the transient dilation process with limited creation of open space (Jebrak, 1997) within the fault-hosted veins.

This change in distribution of breccias at different levels of the veins suggests that power of coseismic hydrothermal brecciation fluctuated within different levels of a vein during same mineralization event. It means that the brecciation may have affected the entire vein fill proximal to the most vigorous upflow zone close to the level of boiling at lower levels of a vein, while it may have been limited to the footwall contact of the vein more distally at the upper levels of a vein. Alternatively, the change in breccias distribution may be the result of different brittle failure mechanisms caused by the change in mechanical properties of variable vein infill deposited at different levels of a single vein.

Internal evolution of the Karatepe vein is different from the other fault-hosted veins as shown by its different infill characteristics (Figures 4a and 4c). (i) The absence of crackle to mosaic, and chaotic breccias within the vein, and (ii) formation of laminated-crustiform chalcedony support that the vein was developed distal to the boiling levels at the shallower level of the Kestanelik epithermal system without fluid-assisted brecciation. Matrix-supported cockade-textured breccias (p1) (Figures 4a and 4b) suggest formation by crustiform chalcedonic overgrowths around the wall rock clasts while they are suspended within the fluid conduit (fault) during transient rapid fluid flow immediately after coseismic rupture. The absence of any grading in the clasts of the cockade breccias (Gülyüz et al., 2018) suggests that both shaking (brecciation occurred due to coseismic rupturing) and fluidisation (hydraulic fracturing at depth caused transportation of the clasts to the shallower levels) may have played a role in the formation of the cockade breccias (c.f. Frenzel and Woodcock, 2014). The sharp macroscopic contact between the two mineralization phases (Figure 4a), the absence of fluid-assisted brecciation and microscopically observed cataclasite of p1 chalcedony cemented by p2 chalcedony (Gülyüz et al., 2018) suggest that the vein reopening is not associated with highly dynamic rupturing and vigorous hydrothermal eruption events as in other fault hosted

	Explanation	Representative photo	HW margin	Vein core	FW margin
E-W trending fault-hosted veins	**Matrix supported breccias of wall rocks** Clasts - Wall rocks schist and QFH porphry - Poorly-sorted - Angular to sub-angular Matrix - Saccharoidal-lattice bladed-massive quartz - >70%	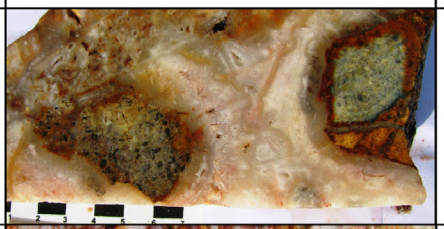	✓	✓	
	Crackle to mosaic breccias Clasts - Saccharoidal-lattice bladed-massive quartz, wall rocks schist and QFH porphyry - Poorly- to good-sorted - Angular to sub-rounded Matrix - Massive quartz ± hematite - ~20-80%		✓	✓	✓
	Crackle to chaotic breccias Clasts - Saccharoidal,lattice bladed,massive quartz - Poorly-sorted - Angular to sub-rounded Matrix - Massive quartz-hematite - <20%		✓	✓	✓
NE-SW to NNE-SSW trending extensional veins	**Matrix supported breccias of wall rock** Clasts - Wall rock schist - Poorly- to good-sorted - Angular to sub-angular Matrix - Saccharoidal-lattice bladed quartz - >50%		✓		✓
	Crackle to mosaic breccias Clasts - Saccharoidal and massive quartz, wall rock schist, earlier vein infill(s) (breccia in breccia) - Poorly-sorted - Angular to sub-rounded Matrix - Massive quartz-hematite - ~20-70%	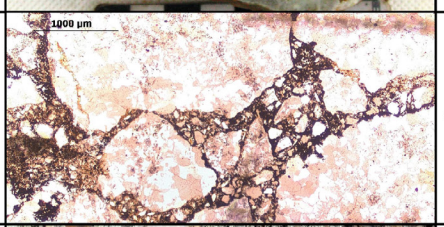	✓	✓	✓
	Crackle to chaotic breccias Clasts - Saccharoidal, lattice bladed, and massive quartz - Poorly-sorted - Angular to sub-rounded Matrix - Massive quartz-hematite - <50%		✓	✓	✓
NNE-SSW trending Topyurt Vein	**Mosaic to chaotic breccias** Clasts - Earlier vein infill(s) (breccia in breccia) - Poorly-sorted - Angular to sub-rounded Matrix - Massive quartz-hematite - ~40%	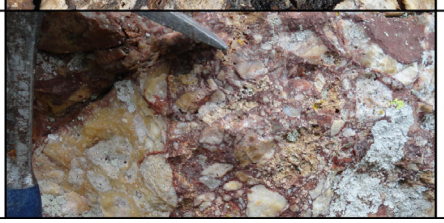	✓	✓	✓

Figure 9. Characteristics of breccia types observed in the Kestanelik epithermal veins. A representative photo is provided for each breccia type. Tick marks indicate the locations of each breccia type within vein.

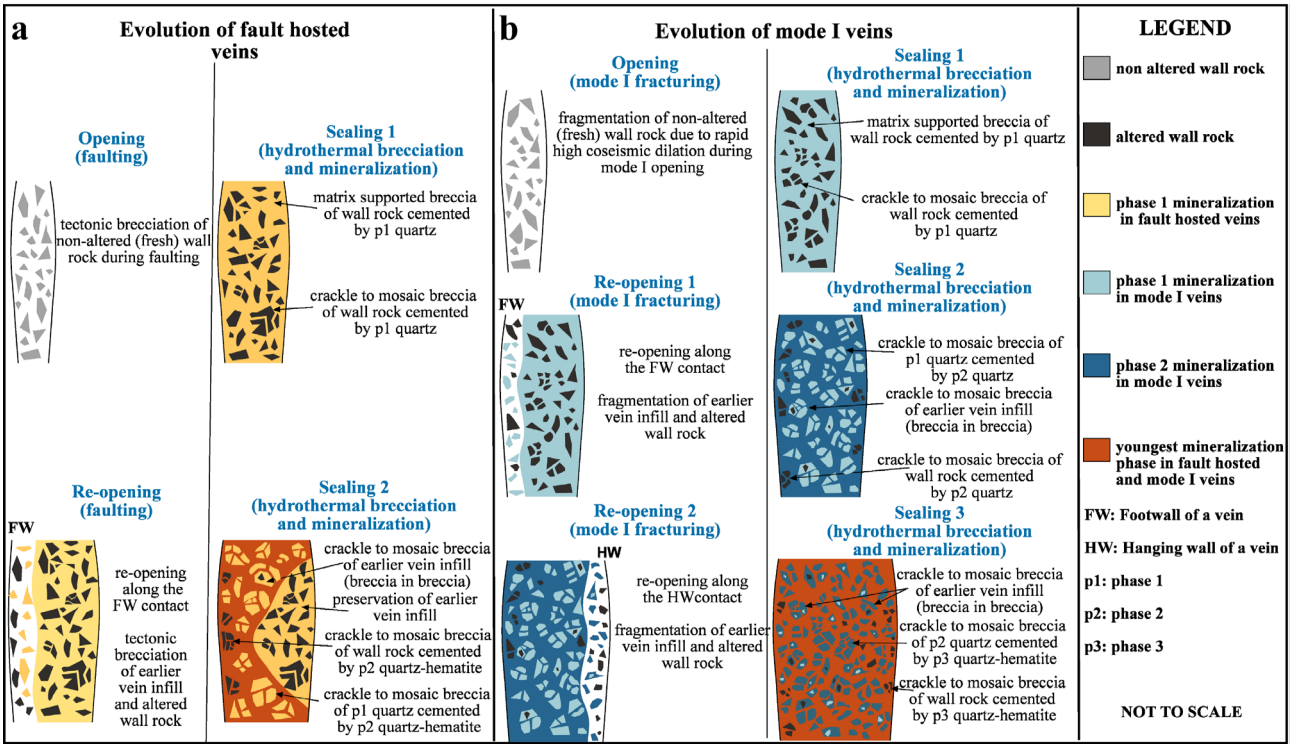

Figure 10. (a) Hypothetical model for internal structural evolution of fault-hosted veins by repeated opening (faulting) and sealing (mineralization) events. (b) Hypothetical structural model for internal evolution of mode I veins by repeated opening (mode I fracturing) and sealing (mineralization) events (see the text for detailed explanation).

veins, and phase 2 crustiform chalcedony (Figure 4a) developed as gradual open space fill after the vein was reopened along its FW margin. The low average Au content (0.461 g/t) of the vein is attributed to its development at the shallower level of the epithermal system by fluids that already released most of its metal load at deeper parts.

During a seismic event, reopening of a clogged mode I vein along the either margin of the vein (Gülyüz et al., 2018) causes fragmentation of previous vein infill and wall rock due to high coseismic dilation (Figure 10b). Commonplace of (i) matrix supported breccias with angular to subangular clasts of wall rock schist cemented by later phases of quartz generations (Figures 6a, and 7d, 7e) as clasts within younger breccias, and (ii) crackle to mosaic breccias with clasts of wall rock schist and previous vein infill(s) (Figure 7h) cemented by massive micro-crystalline quartz-hematite close to vein margins confirms the rupturing along either margins, the HW or FW of the veins, and derivation of wall rock at each cycle of reopening associated fragmentation phase (Figures 10b and 11). Rapid high coseismic dilation initiates flashing and associated hydrothermal brecciation within the veins. Observation of crackle to mosaic breccias with a matrix of massive micro-crystalline quartz-hematite cementing the clasts of (i) quartz belonging to earlier vein phases (Figures 7f and 7h) and (ii) breccia of earlier vein infill (breccia in breccia) (Figure 7g) indicate reworking of earlier vein breccia phases by repeated coseismic dilatant fracturing and subsequent fluid-assisted hydrothermal brecciation (Figures 10b and 11).

Chaotic polymictic breccias cemented by the youngest phase of quartz generation along with hematite (massive quartz±hematite) are observed at the uppermost levels of most of the veins (both fault-hosted and mode I veins) (Figure 11). The presence of angular to subrounded, polymictic clasts displaying various textures representing different phases of quartz generations in these breccias (Figures 5f, 5g, 5h, and 8a) suggests transportation of the clasts to the upper levels of the veins where more dilation due to lower confining pressure exists. The reason behind this transportation might be explained by a hydrodynamic action resulted from the vigorous boiling of hydrothermal fluids associated with abrupt fluid pressure-drop during the seismic-slip. Alternatively, the common subrounded nature of the clasts suggests fragment-on-fragment impact brecciation, which together with the massive nature of the quartz±hematite matrix suggest occurrence by rapid dilation as expansion-related implosion brecciation (Jebrak, 1997; Rhys et al., 2020). These chaotic polymictic breccias also resemble the breccias observed at the

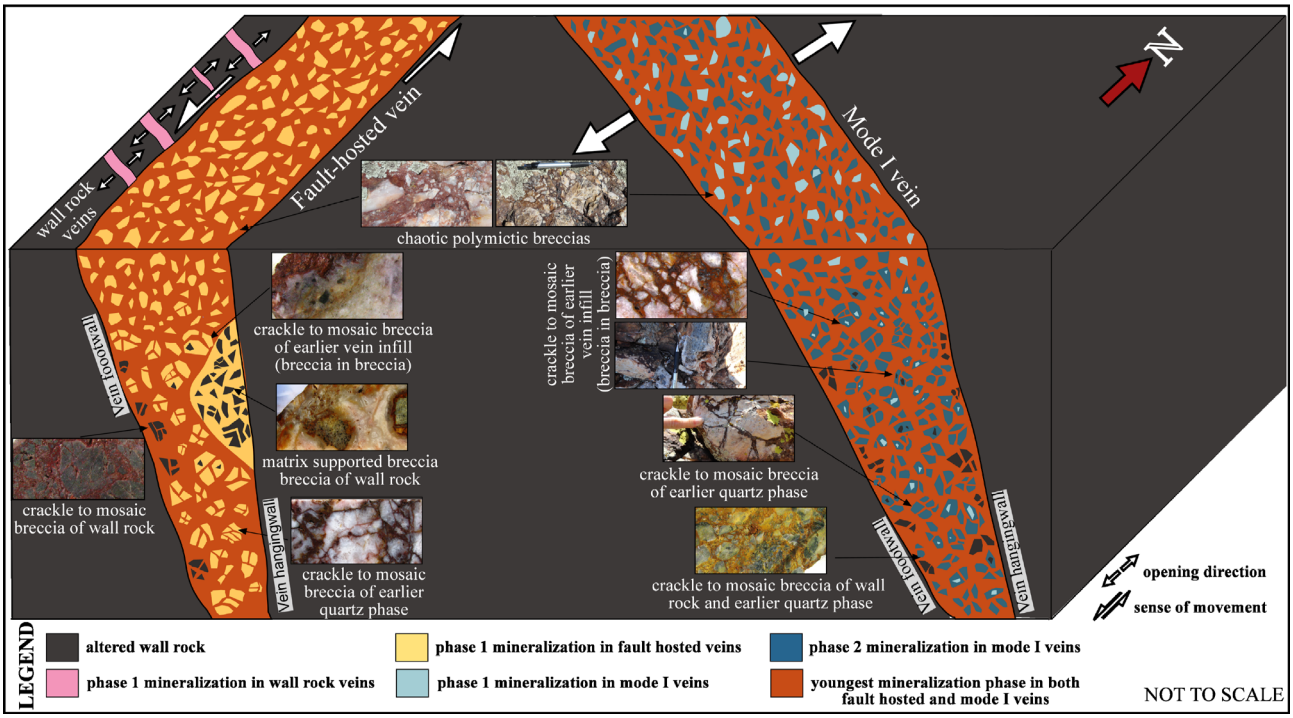

Figure 11. Hypothetical block diagram summarizing the trend, breccia characteristics and filling of fault-hosted and mode-I veins together with wall rock veins peripheral to the fault hosted veins (see the text for detailed explanation).

uppermost parts of the breccia pipes found in some hydrothermal deposits (e.g., Tamaş and Milesi, 2003). The chaotic breccias are correlated with high grade gold values.

5.2. Multiphase mineralization

Multiple phases of deformation caused by repeated cycles of earthquake rupturing, hydrothermal brecciation, and associated fluid flow result in multiphase mineralization at Kestanelik. Temporal relations between vein textures and breccias at the Kestanelik veins are summarized in Figure 12. This figure illustrates (i) two phases of mineralization in the Karatepe, K2, K3 veins (Figures 4c and 5a), (ii) three phases of mineralization in the KK2, KK4, K1 (Figures 7a, 7b, and 7c) and Topyurt veins (Figures 8b, 8c, and 8d), and (iii) four phases of mineralization in the KK1 and KK3 veins (Figures 6f, 6g, and 6h). On the other hand, only one phase of mineralization is identified on the extensional damage zone veins and sheeted veins (Figures 8f, 8g, and 8h). A varying number of mineralization events for the veins proposes that any individual earthquake event-a major seismic event involving multiple fault-slip episodes-may have affected only one or two veins (or more), but not all at once. This means that, during any one earthquake event, while some sealed veins reopened, some veins remained sealed. As a result, the location of the main boiling event shifted both laterally and vertically through time according to which veins the earthquake-related dilation and associated fluid pressure drop occurred. Paleoseismic studies also show that repeated earthquakes reoccupy a narrow zone and that individual paleoseismic zones are reused by different earthquakes (e.g., Gomez et al., 2003). Similarly, observations of repeated spring (CO_2-charged) reactivation (Burnside et al., 2013) and mineralization distribution (Hammond and Evans, 2003) show that only a small part of an individual fault system is active at any one time. Rupturing on different veins may also tap into different reservoirs of hydrothermal fluids, and results in different ratios of fluid-wall rock interaction, and/or mixing of hydrothermal fluid and meteoric water in different ratios. However, the full implications of the different number of mineralization events are yet to be explored and are beyond the scope of this study. Stable isotopes (O, H, and C) and fluid inclusion analyses could be used to investigate the varying fluid sources, mixing and fluid-wall rock ratios (e.g., Urquhart, 2011) in (i) infills of different veins and (ii) in different generations of fill in a single vein.

It is also remarkable here that two phases of mineralization are defined from the fault-hosted veins while mode I veins host at least three mineralization phases (Figure 12). Although faults typically control more of the fluid flow in epithermal systems (e.g., Sibson et al., 1975; Oliver, 2001), fault-hosted veins record fewer mineralization events than the mode I veins at Kestanelik (Figure 12). Two different alternative scenarios can be proposed for this contradiction as explained below.

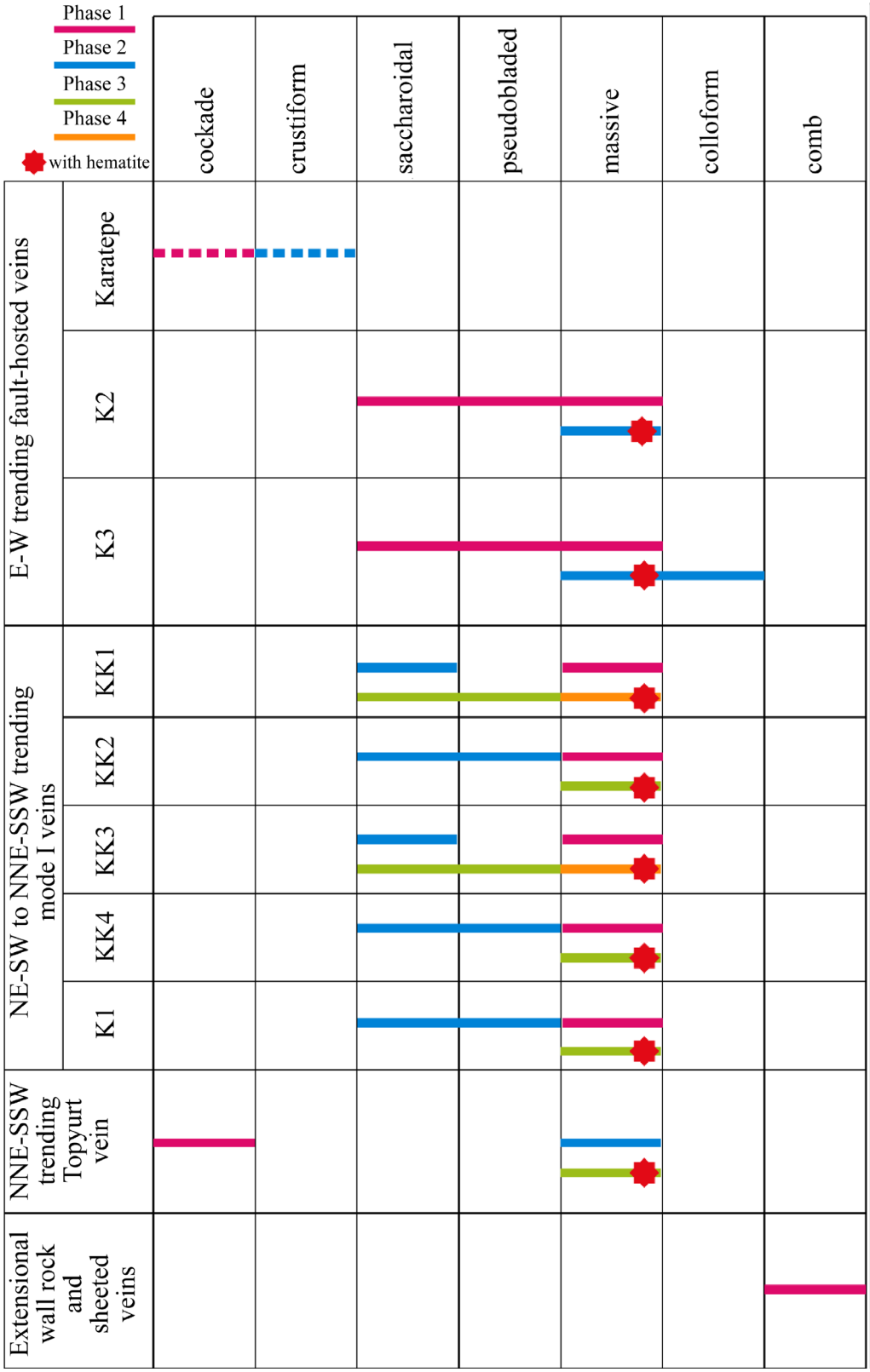

Figure 12. Different mineralization phases and associated vein quartz textures detected from each vein based on cross cutting relationships among vein textures and breccias. Dashed line indicates chalcedony while solid line indicates quartz. Red star represents quartz phases associated with hematite.

Firstly, although the fault-hosted veins were completely sealed, the flow may have continued through the still-open conduits of mode I veins. Because mode I fractures accommodate more dilation compared to faults, which causes high fluid flux to focus the conduits of mode I veins. Secondly, after all of the Kestanelik veins were completely sealed, overpressured fluid system might have been developed due to low permeability nature of the Kestanelik host rocks QFH porphyry and schist. In this case, fluid pressurization occurs faster relative to the tectonic loading rates (Cox, 2020). At low differential stresses, like in epithermal systems developed at shallow crustal settings, fluid pressurization can drive extensional failure but not shear failure (Cox, 2020). This may explain why fault-hosted veins remained sealed while mode I veins were reopened and hosted more fluid flow and associated mineralization events.

Although fault-hosted veins record fewer mineralization events, the average Au content of the fault-hosted veins (4.106 g/t) is higher than that of mode I veins (2.736 g/t). However, economic gold mineralization is not restricted to mode I veins and both vein types contain economic gold mineralization.

Although the fault hosted veins in Kestanelik have more than one phase of mineralization (Figures 4c and 5a), damage zone structures (extensional wall rock veins) only host one phase of mineralization (Figures 8f, 8h, and 12). This result seems to contradict the suggestion that damage zone structures have higher permeability than the individual fault segments (Cox, 2005) and they may host multiple episodes of successive brittle failure events (Caine et al., 1996). Two different explanations may be proposed to explain the case at the Kestanelik deposit; (1) Fault zones were a localized barrier (Caine et al., 1996) meaning that the fault core itself was well-developed while the damage zone structures were absent or poorly developed to be permeable during earlier rupture events. But they latterly developed and became permeable by repeated ruptures and then hosted only one phase of mineralization in the latest rupture event. (2) The damage zone structures were sealed and deactivated during the following rupture events and hosted only one phase of mineralization. The lack of reopening of the damage zone structures may be due (i) to the rotation of the optimum stress field for reopening these structures by transient stress variation (Gülyüz et al., 2018), or (ii) to a strong mechanical contrast at the boundary of these veins being a more effective location for future slip (e.g., Cox, 2005). In either case, some damage zone structures must have been sealed after the main fault hosted veins were present because some of the damage zone veins curve towards the main vein. This curvature is most likely due to the competency difference between the vein quartz and adjacent altered host rock. To sum up, damage zone structures adjacent to the main fault seem to only host one phase of mineralization and seal after the main fault is completely sealed. It has been suggested that more protracted fluid flow occurs through damage zone structures compared to the main fault which is sealed rapidly (Micklethwaite and Cox, 2004; 2006; Sheldon and Micklethwaite, 2007). However, there is no evidence from the textures in the wall rock veins of that is the case.

Since these extensional veins form and seal after the adjacent faults were completely sealed, an alternative scenario to explain why these veins host only one phase of mineralization can be suggested for their origin. These veins may have been formed as hydraulic extension fractures by fluid pressurization rather than tectonic loading at low differential stress conditions (Cox, 2020) after permeability was lost due to the complete sealing of the major vein conduits at the waning stage of the epithermal system.

Extensional sheeted veins at the deepest part of the epithermal system also contain one mineralization phase, although the major veins above them reflect multiphase mineralization. Sheeted veins may have sealed and deactivated during any time of the epithermal system due to the shifting of the paleoactive plumbing conduits as the epithermal system evolved. Their high gold content is most likely related to their formation at the deepest part of the epithermal system just above the boiling level where hydrothermal fluid release most of its gold load.

6. Conclusions

The evolution of epithermal systems is complicated due to the multiple pulses of fluid flow and mineralization events associated with repeated deformation and permeability enhancement processes in upper crustal brittle settings. Studying the textures and structures preserved in the vein record is a powerful tool for studying the complicated 4D evolution of epithermal veins.

Detailed study of vein textures and breccias of the Kestanelik epithermal Au-Ag deposit has reached the following:

- Fault-hosted veins and mode I veins share many textural and breccia characteristics that are attributed to the (i) overprinting of tectonic breccias formed during coseismic rupturing by subsequent coseismic hydrothermal brecciation and (ii) reworking of earlier vein breccia phases by repeated rupture and associated hydraulic fracturing events.
- Hydrothermal brecciation triggered by coseismic fluid pressure drop after the reactivation of the sealed faults along the vein footwall-wall rock contact during an earthquake event causes partial brecciation of previous

vein infill close to the footwall margin of the vein, and brecciation of the wall rock adjacent to the footwall of the vein at upper levels of the veins, but complete brecciation of the infill, and brecciation of the wall rock adjacent to the vein margins. This proposes that the power of coseismic hydrothermal brecciation is controlled by the distance to the level of vigorous boiling within different levels of a vein during the same mineralization event meaning that the brecciation affects the entire vein proximal to the most vigorous upflow zone close to the level of boiling at lower levels of a vein, while it is limited to the footwall contact of the vein more distally at the upper levels of a vein.

· Chaotic polymictic breccias cemented by the youngest mineralization phase quartz±hematite observed at the uppermost parts of the most veins are interpreted as the result of upward transportation of the clasts to the shallower levels of the veins by the hydrodynamic action of boiling fluids. These breccias contain high grade gold values.

· Different number of mineralization events (two, three, or four) picked up from the veins imply that any earthquake event does not affect (reopen) all of the veins at once and location of the main boiling event shifted through time which may have tapped into different reservoirs of hydrothermal fluids.

· Fault-hosted veins record two phases of mineralization while mode I veins host at least three mineralization events suggesting that high fluid flux focused into conduits of mode I veins that accommodate more dilation. In addition, mode-I veins may have been reopened due to the driven of extensional failure rather than shear failure under low differential stresses by fluid pressurization after all Kestanelik veins were completely sealed.

· While fault-hosted veins have fewer mineralization events, their average gold grade is higher compared to that of mode I veins.

· Fault-hosted veins have more than one phase of mineralization, but associated damage zone structures only host one phase of mineralization contradicting the suggestion that damage zone structures have higher permeability and may host multiple episodes of brittle failure and mineralization events.

· Fewer mineralization events in damage zone structures compared to the adjacent faults are attributed to (i) the absence or poor development of the damage zone structures in earlier seismic events or (ii) deactivation of them after clogging due to the rotation of the optimum stress field, or (iii) their formation as hydraulic extension fractures at the waning stage of the epithermal system.

Acknowledgements

This paper is a part of a PhD study carried out at the University of Strathclyde with University of Strathclyde scholarship and financial support of Geochemico Incorporated. The study benefited from discussions with Nuretdin Kaymakcı, Richard A. Lord, and Erhan Gülyüz. The authors acknowledge Chesser Resources for providing accommodation and logistics for fieldwork, and access to drill core data. We gratefully thank C.S. Yüceer, M. Çetintaş, geologists and staff at Kestanelik for their help, and Erhan Gülyüz for his generous help in all phases of the fieldwork. Last, we appreciate the late David R. Gladwell for providing financial support from Geochemico Incorporated and help during the fieldwork.

Conflict of interest

The authors have no conflict of interest to declare.

References

Altunkaynak Ş, Genç ŞC (2008). Petrogenesis and time-progressive evolution of the Cenozoic continental volcanism in the Biga Peninsula, NW Anatolia (Turkey). Lithos 102: 316–340. https://doi.org/10.1016/j.lithos.2007.06.003

Banks DA, Bozkaya, G, Bozkaya, Ö (2019). Direct observation and measurement of Au and Ag in epithermal mineralizing fluids. Ore Geology Reviews 111: 1-16. https://doi.org/10.1016/j.oregeorev.2019.102955

Brown, KL (1986). Gold deposition from geothermal discharges in New Zealand. Economic Geology 81: 979-988. https://doi.org/10.2113/gsecongeo.81.4.979

Buchanan LJ (1981). Precious metal deposits associated with volcanic environments in the southwest. In: Dickson WR, Payne WD (editors). Relations of Tectonics to Ore Deposits in the Southern Cordillera: Arizona Geological Society Digest, pp. 237-262.

Burnside NM, Shipton ZK, Dockrill B, Ellam RM (2013). Man-made versus natural CO_2 leakage: A 400 k.y. history of an analogue for engineered geological storage of CO_2. Geology 41: 471–474. https://doi.org/10.1130/G33738.1

Caine JS, Evans J, Forster C (1996). Fault zone architecture and permeability structure. Geology 24: 1025–1028. https://doi.org/10.1130/0091-7613(1996)024%3C1025:FZAAPS%3E2.3.CO;2

Caine JS, Bruhn RL, Forster CB (2010). Internal structure, fault rocks, and inferences regarding deformation, fluid flow and mineralization in the seismogenic Stillwater normal fault, Dixie Valley, Nevada. Journal of Structural Geology 32: 1576-1589. https://doi.org/10.1016/j.jsg.2010.03.004

Chauvet A, Bailly L, Andre A, Monie P, Cassard D, Tajada, FL, Vargas JR, Tuduri J (2006). Internal vein texture and vein evolution of the epithermal Shila-Paula district, southern Peru. Mineralium Deposita 41: 387-410. https://doi.org/10.1007/s00126-006-0068-4

Chauvet A (2019). Structural controls of ore deposits: The role of pre-existing structures on the formation of mineralised vein systems. Minerals 9 (1): 56. https://doi.org/10.3390/min9010056

Cowan DS (1999). Do faults preserve a record of seismic slip? A field geologist's opinion. Journal of Structural Geology 21: 995-1001. https://doi.org/10.1016/S0191-8141(99)00046-2

Cox S (2005). Coupling between Deformation, Fluid Pressures, and Fluid Flow in Ore-Producing Hydrothermal Systems at Depth in the Crust. Economic Geology 100: 39-75. https://doi.org/10.5382/AV100.04

Cox S (2010). The application of failure mode diagrams for exploring the roles of fluid pressure and stress states in controlling styles of fracture-controlled permeability enhancement in faults and shear zones. Geofluids 10: 217-233. https://doi.org/10.1111/j.1468-8123.2010.00281.x

Cox S, Sun SS, Etheridge MA, Wall VJ, Potter TF (1995). Structural and geochemical on the development of turbidite-hosted gold-quartz vein deposits, Wattle Gully mine, central Victoria, Australia. Economic Geology 14: 1-24. https://doi.org/10.2113/gsecongeo.90.6.1722

Cox S, Knackstedt M, Braun J (2001). Principles of structural control on permeability and fluid flow in hydrothermal systems. Reviews in Economic Geology 14: 1-24. https://doi.org/10.5382/Rev.14.01

Cox S (2020). The dynamics of permeability enhancement and fluid flow in overpressured, fracture-controlled hydrothermal systems. In Rowland JV, Rhys DA (editors) Reviews in Economic Geology, v.21, Applied Structural Geology of Ore-forming Hydrothermal Systems: Society of Economic Geologists Inc, pp. 25-82.

Dong G, Morrison, G, Jaireth S (1995). Quartz textures in epithermal veins, Queensland— classification, origin, and implication. Economic Geology 90: 1841–1856. https://doi.org/10.2113/gsecongeo.90.6.1841

Dowling K, Morrison GW (1989). Applications of quartz textures to the classification of gold deposits using North Queensland examples. Economic Geology Monograph 6: 342-355. https://doi.org/10.5382/Mono.06.26

Frenzel M, Woodcock NH (2014). Cockade breccia: product of mineralisation along dilational faults. Journal of Structural Geology 68: 194-206. https://doi.org/10.1016/j.jsg.2014.09.001

Gomez F, Meghraoui M, Darkal AN, Hijazi F, Mouty M et al. (2003). Holocene faulting and earthquake recurrence along the Serghaya branch of the Dead Sea fault system in Syria and Lebanon. Geophysical Journal International 153: 658-674. https://doi.org/10.1046/j.1365-246X.2003.01933.x

Gülyüz N (2017). Textural and structural characteristics of the Kestanelik epithermal vein system, NW Turkey, implications for permeability enhancement mechanisms and gold exploration in epithermal systems. PhD, University of Strathclyde, Glasgow, UK.

Gülyüz N, Shipton ZK, Kuşcu İ, Lord RA, Kaymakcı N et al. (2018). Repeated reactivation of clogged permeable pathways in epithermal gold deposits: Kestanelik epithermal vein system, NW Turkey. Journal of the Geological Society 175: 509–524. https://doi.org/10.1144/jgs2017-039

Gülyüz N, Gülyüz E, Shipton ZK, Kuşcu İ, Lord RA (2020). Geological and mineralization characteristics of the Kestanelik epithermal Au-Ag deposit in the Tethyan Metallogenic Belt, NW Turkey. Geosciences Journal 24: 407-424. https://doi.org/10.1007/s12303-019-0030-y

Hammond KJ, Evans JP (2003). Geochemistry, mineralization, structure, and permeability of a normal-fault zone, Casino mine, Alligator Ridge district, north central Nevada. Journal of Structural Geology 25(5): 717-736. https://doi.org/10.1016/S0191-8141(02)00060-3

Hedenquist JW, Lowenstern JB (1994). The role of magmas in the formation of hydrothermal ore deposits. Nature 370: 519-527. https://doi.org/10.1038/370519a0

Hedenquist JW, Arribas MA, Gonzalez-Urien E (2000). Exploration for epithermal gold deposits. Reviews in Economic Geology, 13: 245-277. https://doi.org/10.5382/Rev.13.07

Henley RW (1985). The geothermal framework of epithermal deposits. Reviews in Economic Geology 2: 1-24. https://doi.org/10.5382/Rev.02.01

Henley RW, Berger B (2000). Self-ordering and complexity in epizonal mineral deposits. Annual Review of Earth and Planetary Sciences 28: 669-719. https://doi.org/10.1146/ANNUREV.EARTH.28.1.669

Hulin CD (1929). Structural control of ore deposition. Economic Geology 24: 15-49. https://doi.org/10.2113/gsecongeo.24.1.15

Kuşcu İ, Tosdal R, Gençalioğlu-Kuşcu G (2019). Episodic porphyry Cu (Mo-Au) formation and associated magmatic evolution in Turkish Tethyan Collage. Ore Geology Reviews 107: 119-154. https://doi.org/10.1016/j.oregeorev.2019.02.005

Masoch S, Fondriest M, Preto N, Secco M, Toro GD (2019). Seismic cycle recorded in cockade-bearing faults (Col de Teghime, Alpine Corsica). Journal of Structural Geology 129: 103889. https://doi.org/10.1016/j.jsg.2019.103889

McKay L, Shipton ZK, Lunn R, Andrews B, Raub TD et al. (2019). Detailed Internal Structure and Along-Strike Variability of the Core of a Plate Boundary Fault: The Highland Boundary Fault, Scotland. Journal of the Geological Society 177: 283-296. https://doi.org/10.1144/jgs2018-226

Micklethwaite S, Cox S (2004). Fault-segment rupture, aftershock-zone fluid flow, and mineralisation. Geology 32: 813-816. https://doi.org/10.1130/G20559.1

Micklethwaite S, Cox S (2006). Progressive fault triggering and fluid flow in aftershock domains: Examples from mineralized Archean fault systems. Earth and Planetary Science Letters 250: 318-330. https://doi.org/10.1016/j.epsl.2006.07.050

Micklethwaite S (2009). Mechanisms of faulting and permeability enhancement during epithermal mineralisation: Cracow goldfield, Australia. Journal of Structural Geology 31: 288-300. https://doi.org/10.1016/j.jsg.2008.11.016

Moncada D, Mutchler S, Nieto A, Reynolds TJ, Rimstidt JD et al. (2012). Mineral textures and fluid inclusion petrography of the epithermal Ag-Au deposit at Guanajuato, Mexico: Application to exploration. Journal of Geochemical Exploration 114: 20-35. https://doi.org/10.1016/j.gexplo.2011.12.001

Okay AI. Tüysüz O (1999). Tethyan sutures of northern Turkey. In B. Durand, L. Jolivet F Horváthand, Séranne M (editors). The Mediterranean Basins: Tertiary extension within the Alpine orogeny: Geological Society of London, pp. 475–515.

Okay AI, Siyako M, Bürkan KA (1990). Geology and tectonic evolution of the Biga Peninsula. Bulletin of the Turkish Association of Petroleum Geologists 2: 83–121 (in Turkish with English abstract)

Okay AI, Satır M, Maluski H, Siyako M, Monie P et al. (1996). Paleo- and Neo-Tethyan events in northwest Turkey: geological and geochronological constraints. In Yin A, Harrison M (editors). Tectonics of Asia: Cambridge University Press, pp. 420-441.

Oliver NHS (2001). Linking of regional and hydrothermal systems in the mid-crust by shearing and faulting. Tectonophysics 335: 147-161. https://doi.org/10.1016/S0040-1951(01)00054-3

Rhys DA, Lewis PD, Rowland JV (2020). Structural controls on ore localization in epithermal gold-silver deposits: a mineral systems approach. In JV Rowland, Rhys DA (editors), Reviews in Economic Geology, v.21, Applied Structural Geology of Ore-forming Hydrothermal Systems: Society of Economic Geologists Inc, pp: 83-145.

Rowe CD, Griffith WA (2015). Do faults preserve a record of seismic slip: A second opinion. Journal of Structural Geology 78: 1-26. https://doi.org/10.1016/j.jsg.2015.06.006

Sanchez-Alfaro P, Reich M, Driesner T, Cembrano J, Arancibia G et al. (2016). The optimal windows for seismically-enhanced gold precipitation in the epithermal environment. Ore Geology Reviews 79: 463-473. https://doi.org/10.1016/j.oregeorev.2016.06.005

Saunders JA (1994). Silica and gold textures in bonanza ores of the Sleeper deposit, Humboldt County, Nevada: Evidence for colloids and implications for epithermal ore-forming processes. Economic Geology 89 (3): 628-638. https://doi.org/10.2113/gsecongeo.89.3.628

Sheldon HA, Micklethwaite S (2007). Damage and permeability around faults: Implications for mineralization. Geology, 34, 903–906. https://doi.org/10.1130/G23860A.1

Shikazano N, Shimizu M (1987). The Ag/Au ratio of native gold and electrum and the geochemical environment of gold vein deposits in Japan. Mineralium Deposita 22: 309-314. https://doi.org/10.1007/BF00204524

Shimizu T (2014). Reinterpretation of quartz textures in terms of hydrothermal fluid evolution at the Koryu Au-Ag deposit, Japan. Economic Geology 109: 2051-2065. https://doi.org/10.2113/econgeo.109.7.2051

Sibson RH, Moore JMcM, Rankın AH (1975). Seismic pumping – a hydrothermal fluid transport mechanism. Journal of the Geological Society 131 (6): 653-659. https://doi.org/10.1144/gsjgs.131.6.0653

Sibson RH (1987). Earthquake rupturing as a mineralizing agent in hydrothermal systems. Geology 15: 701–704. https://doi.org/10.1130/0091-7613(1987)15%3C701:ERAAMA%3E2.0.CO;2

Sibson RH (1992). Implications of fault-valve behavior for rupture nucleation and recurrence. Tectonophysics 18: 1031-1042. https://doi.org/10.1016/0040-1951(92)90065-E

Sibson RH (2001). Seismogenic framework for hydrothermal transport and ore deposition. Reviews in Economic Geology 14: 25-50. https://doi.org/10.5382/Rev.14.02

Sillitoe RH, Hedenquist JW (2003). Linkages between volcanotectonic settings, ore-fluid compositions, and epithermal precious metal deposits. Society of Economic Geologists Special Publications 10. https://doi.org/10.5382/SP.10.16

Simmons SF, White NC, John D (2005). Geological characteristics of epithermal precious and base metal deposits. *E*conomic Geology 100th Anniversary Volume: 485-522. https://doi.org/10.5382/AV100.16

Spurr JE (1925). Ore magmas versus magmatic waters. Engineering and Mining Journal 119: 890.

Strujkov SF, Ryjıvi OB, Aristov VV (1996). Geological structure and ore mineralogy of the Julietta gold-silver deposit, northeast Russia. International Geology Review 38: 625-648. https://doi.org/10.1080/00206819709465350

Tamas CG, Mılesi JP (2003). Hydrothermal breccia pipe structures-General features and genetic criteria- II. Phreatic breccias. Geologia 1: 55-66.

Tarasewicz JPT, Woodcock NH, Dickson JAD (2005). Carbonate dilation breccias: Examples from the damage zone to the Dent Fault, northwest England. GSA Bulletin 117: 736-745. https://doi.org/10.1130/B25568.1

Tümad Madencilik ve Sanayi A.Ş. (n.d.) Lapseki Altın ve Gümüş Madeni. https://www.tumad.com.tr/lapseki-altin-ve-gumus-madeni (in Turkish).

Türkecan A, Yurtsever A (2002). *1:500 000 scale geological map of Turkey, İstanbul sheet.* General Directorate of Mineral Research and Exploration publications, Ankara.

Urquhart ASM (2011). Structural controls on CO_2 leakage and diagenesis in a natural long-term carbon sequestration analogue: Little Grand Wash fault, Utah, PhD, The university of Texas at Austin, USA.

White NC, Hedenquist JW (1995). Epithermal gold deposits: Styles, characteristics and exploration. Society of Economic Geologists Newsletter 23: 9–13

Woodcock NH, Dickson JAD, Tarasewicz JP (2007). Transient permeability and reseal hardening in fault zones: evidence from dilation breccia textures. In Lonergan L, Jolley RJH, Rawnsley K, Sanderson DJ (editors). Fractured Reservoirs: Geological Society London, pp. 43–53.